

VISION-LSTM: xLSTM AS GENERIC VISION BACKBONE

Anonymous authors
Paper under double-blind review

ABSTRACT

Transformers are widely used as generic backbones in computer vision, despite initially introduced for natural language processing. Recently, the Long Short-Term Memory (LSTM) has been extended to a scalable and performant architecture – the xLSTM – which overcomes long-standing LSTM limitations via exponential gating and parallelizable matrix memory structure. In this paper, we introduce Vision-LSTM (ViL), an adaption of the xLSTM building blocks to computer vision. ViL comprises a stack of xLSTM blocks where odd blocks process the sequence of patch tokens from top to bottom while even blocks go from bottom to top.

ViL achieves strong performances on classification, transfer learning and segmentation tasks as well as a beneficial pre-training cost-to-performance trade-off. Experiments show that ViL holds promise to be further deployed as new generic backbone for computer vision architectures.

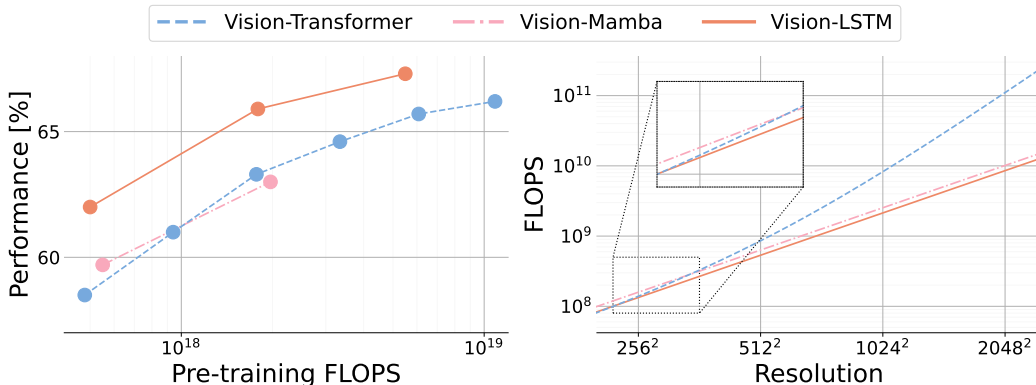


Figure 1: The efficient and scalable design of Vision-LSTM shows strong performances, uses less FLOPS than Transformer/Mamba counterparts and scales linear to higher resolutions. Performance is averaged over ImageNet accuracy, ADE20K mIoU and VTAB-1K accuracy.

1 INTRODUCTION

Language modeling architectures — such as Transformers (Vaswani et al., 2017; Achiam et al., 2023; Team et al., 2023) or more recently State Space Models (Gu et al., 2021; Gupta et al., 2022) such as Mamba (Gu & Dao, 2023) — are commonly adapted to the domain of computer vision to make use of their powerful modeling capabilities. However, in natural language processing, an input sentence is typically encoded into tokens that represent words or common subwords (Bostrom & Durrett, 2020) via a discrete vocabulary. To encode images into a set of tokens, Vision Transformer (Dosovitskiy et al., 2021) (ViT) proposed to group an input image into non-overlapping patches (of e.g. 16x16 pixel), linearly project them into a sequence of so-called patch tokens and add positional information to these tokens. This sequence can then be processed by language modeling architectures.

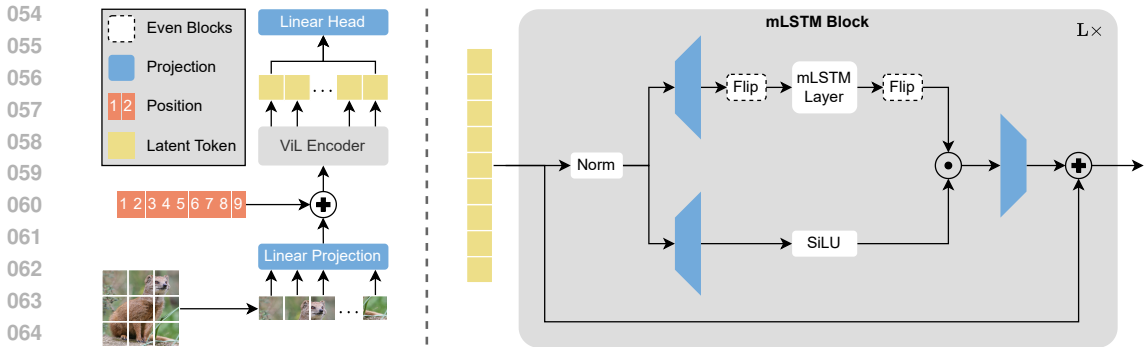


Figure 2: Schematic overview of Vision-LSTM (ViL). Following ViT (Dosovitskiy et al., 2021), an input image is split into patches and linearly projected. Then, a learnable vector is added per position to the patches, producing a sequence of patch tokens. This sequence is then processed by alternating mLSTM blocks where even blocks flip the sequence before and after the mLSTM layer. For classification, ViL uses the concatenation of the first and the last patch as input to a linear classification head. ViL is an isotropic architecture, i.e., all blocks have the same input and output dimension and no downsampling layers are used except the initial patch embedding. Projection layers process each patch individually and the mLSTM exchanges information between patches.

The Extended Long Short-Term Memory (xLSTM) family (Beck et al., 2024) was recently introduced as a new architecture for language modeling. It demonstrates the resurgence of LSTM in the LLM era, performing favorably against the likes of Transformers and State Space Models (SSMs). Analogous to existing vision versions of Transformers or State Space Models, e.g., ViT (Dosovitskiy et al., 2021) or Vision Mamba (Zhu et al., 2024), which have produced great results in various computer vision tasks (Singh et al., 2023; Kirillov et al., 2023; Oquab et al., 2023; Peebles & Xie, 2023; Alkin et al., 2024b), we introduce Vision LSTM (ViL) – a generic computer vision backbone that uses xLSTM blocks as its core components. To adjust xLSTM (an autoregressive model) to computer vision (an often non-autoregressive domain), we employ a stack of alternating mLSTM blocks (Beck et al., 2024) where odd blocks process patches row-wise from top left to bottom right and even blocks go from bottom right to top left. This simple alternating design allows ViL to efficiently process non-sequential inputs, such as images, without introducing additional computations.

Similar to vision adaptations of SSMs (Liu et al., 2024; Zhu et al., 2024; Wang et al., 2024), ViL can exhibit linear computational and memory complexity w.r.t. sequence length which makes it appealing for tasks that benefit from high-resolution images such as medical imaging (Chen et al., 2021; Hatamizadeh et al., 2022; Valanarasu et al., 2021; Xu et al., 2024), segmentation (Kirillov et al., 2023; Cheng et al., 2022), or physics simulations (Bi et al., 2023; Nguyen et al., 2023; Bodnar et al., 2024; Alkin et al., 2024a). In contrast, ViT’s computational complexity scales quadratically due to the self-attention mechanism, rendering them costly to apply to high-resolution tasks.

Our contributions summarize as follows:

- We introduce Vision-LSTM (ViL), an adaption of the mLSTM to computer vision tasks that can serve as a generic vision backbone with linear complexity.
- We show modeling capacity and generalization in the common vision benchmark of pre-training models on ImageNet-1K, followed by fine-tuning on transfer classification and semantic segmentation tasks.
- We ablate various architectural design choices to evaluate their impact on performance and provide insights into the model design.
- We discuss potential future directions and current limitations that, once addressed, will improve ViL even further.

2 METHOD

Vision-LSTM (ViL) introduces xLSTM (Beck et al., 2024) to computer vision, similar to other vision adaptations of sequence modeling architectures, e.g., Vision Transformers (Dosovitskiy et al., 2021), Vision Mamba (Zhu et al., 2024), or Vision RWKV (Duan et al., 2024).

2.1 PRELIMINARIES

In the notation of sequence modeling, we consider a series of input vectors $\mathbf{x}_t \in \mathbb{R}^D$. This series is created by reshaping an image $\tilde{\mathbf{X}} \in \mathbb{R}^{H_I \times W_I \times C_{\text{in}}}$ into a sequence of flattened 2D patches $\tilde{\mathbf{X}} \in \mathbb{R}^{T \times (H_P \cdot W_P \cdot C_{\text{in}})}$ and then projected to $\mathbf{X} \in \mathbb{R}^{T \times D}$ via a shared linear projection. D is the hidden dimension, (H_I, W_I) is the image resolution, C_{in} is the number of image channels, T is the number of patches and (H_P, W_P) is the patch size. After creating a sequence of patches, ViL iteratively refines the features of the patch sequence by processing it with a stack of mLSTM blocks where the sequence is flipped within every second block.

The key innovations of the mLSTM (Beck et al., 2024) are the enhanced storage capacity compared to the classical LSTM (Hochreiter & Schmidhuber, 1997) by using a matrix memory cell $\mathbf{C} \in \mathbb{R}^{d \times d}$ instead of a scalar memory cell $c \in \mathbb{R}$ and introducing exponential gates (instead of sigmoid gates) to the input and forget gates, where d is the hidden dimension within the mLSTM block (typically $d = 2D$).

Intuitively, the mLSTM is a more expressive and faster version of the classical LSTM that can be efficiently parallelized on modern hardware. In ViL, the mLSTM is used to process dependencies between patches, similar to how the attention exchanges information between patches in a ViT. The mLSTM is embedded into a gated MLP architecture, as shown on the right of Figure 2, where the weight matrices of the MLP process each patch individually and the mLSTM exchanges information between patches. For completeness, we outline the forward pass of the mLSTM in the following paragraphs.

The mLSTM (Beck et al., 2024) is a recurrent neural network, which maps a state $(\mathbf{h}_{t-1}, \mathbf{C}_{t-1}, \mathbf{n}_{t-1})$ to a successor state $(\mathbf{h}_t, \mathbf{C}_t, \mathbf{n}_t)$ given input \mathbf{x}_{t-1} . Thereby, $\mathbf{h}_t \in \mathbb{R}^d$ denotes the hidden state, $\mathbf{C}_t \in \mathbb{R}^{d \times d}$ is the cell state and $\mathbf{n}_t \in \mathbb{R}^d$ corresponds to a normalizer state. The full forward pass of the mLSTM is as follows (Beck et al., 2024):

$$\mathbf{C}_t = f_t \mathbf{C}_{t-1} + i_t \mathbf{v}_t \mathbf{k}_t^\top \quad \text{cell state} \quad (1)$$

$$\mathbf{n}_t = f_t \mathbf{n}_{t-1} + i_t \mathbf{k}_t \quad \text{normalizer state} \quad (2)$$

$$\mathbf{h}_t = \mathbf{o}_t \odot \tilde{\mathbf{h}}_t \quad \tilde{\mathbf{h}}_t = \mathbf{C}_t \mathbf{q}_t / \max\{|\mathbf{n}_t^\top \mathbf{q}_t|, 1\} \quad \text{hidden state} \quad (3)$$

$$\mathbf{q}_t = \mathbf{W}_q \mathbf{x}_t + \mathbf{b}_q \quad \text{query input} \quad (4)$$

$$\mathbf{k}_t = \frac{1}{\sqrt{d}} \mathbf{W}_k \mathbf{x}_t + \mathbf{b}_k \quad \text{key input} \quad (5)$$

$$\mathbf{v}_t = \mathbf{W}_v \mathbf{x}_t + \mathbf{b}_v \quad \text{value input} \quad (6)$$

$$i_t = \exp(\tilde{i}_t) \quad \tilde{i}_t = \mathbf{w}_i^\top \mathbf{x}_t + b_i \quad \text{input gate} \quad (7)$$

$$f_t = \exp(\tilde{f}_t) \quad \tilde{f}_t = \mathbf{w}_f^\top \mathbf{x}_t + b_f \quad \text{forget gate} \quad (8)$$

$$\mathbf{o}_t = \sigma(\tilde{o}_t) \quad \tilde{o}_t = \mathbf{W}_o \mathbf{x}_t + \mathbf{b}_o \quad \text{output gate} \quad (9)$$

As exponential activation functions can lead to large activations, the input and forget gates are stabilized with an additional state m_t :

$$m_t = \max(\log(f_t) + m_{t-1}, \log(i_t)) \quad \text{stabilizer state} \quad (10)$$

$$i'_t = \exp(\log(i_t) - m_t) = \exp(\tilde{i} - m_t) \quad \text{stabilized input gate} \quad (11)$$

$$f'_t = \exp(\log(f_t) + m_{t-1} - m_t) \quad \text{stabilized forget gate} \quad (12)$$

As the mLSTM has no memory mixing, i.e, interactions between hidden states from one timestep to the next, it can be fully parallelized for fast computation on modern hardware. For a detailed discussion and theory of the cell state update, further details to the mLSTM we refer to the original work (Beck et al., 2024).

2.2 VISION-LSTM (ViL)

Vision-LSTM (ViL) is a generic backbone for computer vision tasks, which is residually built from mLSTM blocks, as visualized in Figure 2. Following ViT (Dosovitskiy et al., 2021), ViL first splits an image into non-overlapping patches via a shared linear projection, then adds learnable positional embeddings to each patch token. At the core of ViL are alternating mLSTM blocks, which are fully parallelizable and equipped with a matrix memory combined with a covariance update rule. Odd mLSTM blocks process patch tokens from top left to bottom right while even blocks go from bottom right to top left.

Formally, the forward pass of a pair of ViL blocks is:

$$\mathbf{Y}' = \mathbf{X} + \text{Block}_\theta(\mathbf{X}) \quad (13)$$

$$\mathbf{Y} = \mathbf{Y}' + \text{Flip}(\text{Block}_\phi(\text{Flip}(\mathbf{Y}'))) \quad (14)$$

Where “Flip” reverses the sequence and “Block $_\theta$ ” and “Block $_\phi$ ” corresponds to mLSTM blocks with parameters θ and ϕ (shown in Figure 2, right).

A key motivation of ViL is that the autoregressive mLSTM can operate in a recurrent, parallel or chunkwise mode, each with distinct FLOPS and runtime characteristics. Given a sequence length T and hidden dimension d , the complexity of the recurrent mode is $\mathcal{O}(Td^2)$ and needs to be processed sequentially, whereas the parallel mode has complexity $\mathcal{O}(T^2d)$ and is fully parallelizable. The chunkwise mode combines the advantages of the other modes by introducing a chunksize S where the parallel mode is used within chunks and the recurrent mode between chunks. This allows high parallelization, minimal operations and linear scaling with T . Complexity wise, the chunkwise mode has $\mathcal{O}(\frac{T}{S}S^2d + \frac{T}{S}d^2)$ or $\mathcal{O}(TSd + \frac{T}{S}d^2)$ where $\frac{T}{S}$ corresponds to the number of chunks.

3 EXPERIMENTS

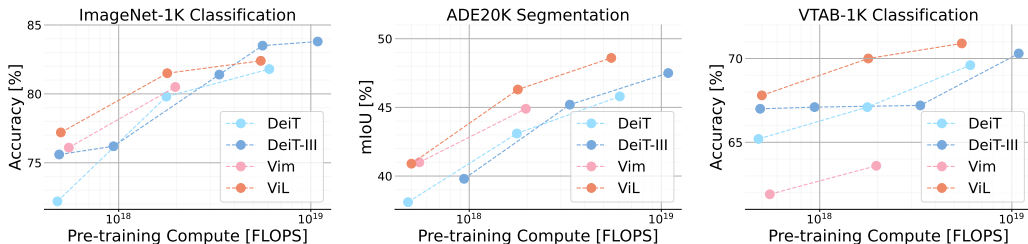


Figure 3: Performance overview of ImageNet-1K pre-trained models in relation to pre-training compute. ViL shows strong performances across classification (ImageNet-1K), semantic segmentation (ADE20K) and transfer classification (VTAB-1K) tasks.

We pre-train models on ImageNet-1K (Deng et al., 2009), which contains 1.3M training images and 50K validation images where each image belongs to one of 1000 classes. ViL models are trained for 800 epochs (tiny) or 400 epochs (small, base) on 192x192 resolution with a learning rate of 1e-3 using a cosine decay schedule. Afterwards, the model is fine-tuned on 224x224 resolution for 20 epochs using a learning rate of 1e-5. Detailed hyperparameters can be found in Appendix Table 10.

We then transfer the pre-trained models to several benchmark tasks: ImageNet-1K classification on the validation set, ADE20K (Zhou et al., 2019) semantic segmentation and

Table 1: ImageNet-1K pre-training accuracy. All models use a patch size of 16x16 with 224x224 resolution at most. Models with “+” in their “Epochs” column pre-train on lower resolution followed by fine-tuning on 224x224 resolution for some epochs. ViL performs favorably against an isotropic convolutional architecture (ConvNeXt) and vision adaptations of transformers (DeiT series), RWKV (VRWKV) and Mamba (Vim, Mamba[®]). Appendix Table 9 confirms these results on OOD and robustness evaluations of these classifiers.

Model	Epochs	#Params	FLOPS	IN-1K
DeiT-T (Touvron et al., 2021a)	300	6M	1.3G	72.2
DeiT-II-T (Touvron et al., 2022a)	400	6M	1.3G	73.5
DeiT-III-T (reimpl.)	800+20	6M	1.3G	76.2
VRWKV-T (Duan et al., 2024)	300	6M	1.2G	75.1
Vim-T (Zhu et al., 2024)	300	7M	1.5G	76.1
Mamba [®] -T (Wang et al., 2024)	280+20	9M	1.6G	77.4
ViL-T	800+20	6M	1.3G	78.3
DeiT-S (Touvron et al., 2021a)	300	22M	4.6G	79.8
DeiT-II-S (Touvron et al., 2022a)	400	22M	4.6G	80.7
DeiT-III-S (Touvron et al., 2022b)	800+20	22M	4.6G	81.4
ConvNeXt-S (<i>iso.</i>) (Liu et al., 2022)	300	22M	4.3G	79.7
VRWKV-S (Duan et al., 2024)	300	24M	4.6G	80.1
Vim-S (Zhu et al., 2024)	300	26M	5.3G	80.5
Mamba [®] -S (Wang et al., 2024)	280+20	28M	5.5G	81.1
ViL-S	400+20	23M	4.7G	81.5
DeiT-B (Touvron et al., 2021a)	300	86M	17.6G	81.8
DeiT-II-B (Touvron et al., 2022a)	400	86M	17.6G	82.7
DeiT-III-B (Touvron et al., 2022b)	800+20	86M	17.6G	83.7
ConvNeXt-B (<i>iso.</i>) (Liu et al., 2022)	300	87M	16.9G	82.0
VRWKV-B (Duan et al., 2024)	300	94M	18.2G	82.0
Mamba [®] -B (Wang et al., 2024)	280+20	99M	20.6G	82.9
ViL-B	400+5	89M	17.9G	82.4

VTAB-1K (Zhai et al., 2019) classification. These benchmarks evaluate global image understanding (ImageNet-1K), semantic local and global understanding (ADE20K) and few-shot generalization to a diverse set of 19 VTAB-1K classification datasets, which include natural images, specialized imagery (medical and satellite) and structured tasks (camera angle prediction, depth estimation, object counting, ...).

Figure 3 shows an overview of performance metrics in relation to total pre-training compute where ViL performs favorably against heavily optimized transformer protocols (DeiT, DeiT-III) and Vision Mamba (Vim). Detailed results are presented in the following sections.

As ViTs are well established in the vision community, they underwent multiple optimization cycles over the years (Dosovitskiy et al., 2021; Touvron et al., 2021a; 2022a; 2021b; 2022b). Therefore, a vast part of the hyperparameter space for pre-training ViTs has been explored. Since this work is the first to apply xLSTM to computer vision, considerably less effort has been put into hyperparameter tuning and architecture optimization, suggesting that future work could improve ViL even further.

3.1 IMAGENET-1K CLASSIFICATION

Table 1 relates parameter counts and FLOPS to validation accuracy after pre-training on ImageNet-1K. ViL outperforms heavily optimized ViT protocols and other backbones on the tiny and small scale. While ViL does not outperform all other models on the base scale, evaluations on downstream tasks (as shown later in Table 2 and Table 3) show that ViL-B still learns strong features, particularly for semantic segmentation and structured tasks.

3.2 ADE20K SEMANTIC SEGMENTATION

Table 2 shows results for transferring ImageNet-1K pre-trained models to ADE20K (Zhou et al., 2019) semantic segmentation using UperNet (Xiao et al., 2018). Also here, ViL shows

strong performances across the board, even outperforming DeiT-III-B despite the lower ImageNet-1K accuracy of ViL-B. The high resolution of the ADE20K segmentation task (512x512) results in a total of 1024 patch tokens where the quadratic complexity of self-attention is significantly more expensive than the linear complexity of the mLSTM, resulting in much fewer FLOPS for ViL. Additionally, the efficient alternating block design results in lower FLOPS than Mamba-based vision models (which also have linear complexity).

Table 2: Semantic segmentation results on ADE20K (Zhou et al., 2019) using UperNet (Xiao et al., 2018). We report mean intersection over union (mIoU) and pixelwise accuracy (ACC) for single- and multi-scale evaluation. Models are trained for 160K updates with a batchsize of 16 on 512x512 resolution. We use a feature pyramid consisting of rescaled feature maps after the 4th, 6th, 8th and final block. Detailed hyperparameters are listed in Appendix Table 12. FLOPS are calculated only from the backbone at 512x512 resolution as all models use the same segmentation head.

Model	#Params	FLOPS	Single-scale		Multi-scale	
			mIoU	ACC	mIoU	ACC
DeiT-T	10M	10.4G	38.1	78.2	40.3	79.9
DeiT-III-T	10M	10.4G	39.8	79.2	42.2	80.7
Vim-T	13M	7.7G	41.0	-	-	-
ViL-T	11M	6.6G	41.2	80.2	43.1	81.3
DeiT-S	41M	31.7G	43.1	80.7	45.2	81.8
DeiT-III-S	41M	31.7G	45.2	81.5	46.3	82.3
Vim-S	46M	27.3G	44.9	-	-	-
Mamba [®] -S	56M	27.6G	45.3	-	-	-
ViL-S	42M	24.4G	46.3	82.0	47.9	82.9
DeiT-B	113M	107.0G	45.8	82.1	47.0	82.9
DeiT-III-B	113M	107.0G	47.5	82.6	49.0	83.3
Mamba [®] -B	132M	102.8G	47.7	-	-	-
ViL-B	115M	93.6G	48.6	82.8	49.6	83.3

3.3 VTAB-1K TRANSFER CLASSIFICATION

Table 3: Transfer classification accuracies on the VTAB-1K (Zhai et al., 2019) benchmark using ImageNet-1K pre-trained models. VTAB-1K consists of 19 datasets split into 7 natural, 4 specialized and 8 structured datasets. We show averages per category and the average accuracy over all 19 datasets (Appendix Table 8 lists all individual accuracies). ViL shows strong generalization performance, outperforming heavily optimized ViT protocols and Vim on the full VTAB-1K benchmark. ViL performs exceptionally well on the structured category. We tune the learning rate for each model and dataset on the validation set and report the average testset accuracy over 5 seeds. Appendix Table 11 lists further hyperparameters.

Model	#Params	FLOPS	Natural	Specialized	Structured	Average
DeiT-T	6M	1.3G	69.2	82.0	53.3	65.2
DeiT-III-T	6M	1.3G	71.9	82.6	55.2	67.1
Vim-T	7M	1.5G	68.0	80.7	47.1	61.9
ViL-T	6M	1.3G	73.6	83.4	56.1	68.3
DeiT-S	22M	4.6G	73.3	83.8	53.2	67.1
DeiT-III-S	22M	4.6G	75.0	83.2	52.3	67.2
Vim-S	26M	5.3G	69.6	81.7	49.4	63.6
ViL-S	23M	4.7G	75.3	84.3	58.3	70.0
DeiT-B	86M	17.6G	76.5	85.2	55.7	69.6
DeiT-III-B	86M	17.6G	77.6	84.8	56.6	70.3
ViL-B	89M	17.9G	76.6	84.7	59.1	70.9

Table 3 shows transfer classification results for ImageNet-1K pre-trained models on the VTAB-1K (Zhai et al., 2019) benchmark. VTAB-1K consists of 19 datasets split into 7 natural datasets (such as CIFAR100 (Krizhevsky, 2009) or Caltech101 (Fei-Fei et al., 2006)), 4 specialized datasets (medical imaging (Veeling et al., 2018; Kaggle & EyePacs, 2015) and remote sensing (Helber et al., 2019; Cheng et al., 2017)) and 8 structured datasets (with

tasks such as object counting (Johnson et al., 2017) or binned depth estimation (Geiger et al., 2013)). We follow common practices and tune the learning rate per model and dataset on the validation set followed by training with the best learning rate on the union of train and validation set. The performance metric is the average testset accuracy over 5 seeds. ViL shows strong transfer classification performance outperforming all other models on the average over all 19 datasets. ViL performs particularly well on the structured datasets where ViL-B outperforms DeiT-III-B despite ViL-B having lower ImageNet-1K accuracy.

4 ABLATION STUDIES

We ablate various design choices of ViL by training ViL-T models for 100 epochs on ImageNet-1K in 224x224 resolution, other hyperparameters follow the ones from Section 3 (see also Appendix B.3). We then report the validation accuracy on ImageNet-1K and fine-tune the model on ADE20K to ensure that design choices are not overfitted to classification. We also use a reduced segmentation pipeline where we use a linear segmentation head and train for 40K updates using a batch size of 16 (other hyperparameters follow Appendix 12).

4.1 ARCHITECTURAL DESIGN

We consider various architecture design choices in Table 4.

Table 4: Architecture design ablation studies. **Default settings**

(a) Traversal Directions				(b) QK Convolution		
Directions	IN1K	ADE20K	Convolution	IN1K	ADE20K	
Uni-dir.	72.2	28.6	None	72.3	29.2	
Bi-dir.	73.7	31.7	Causal-Conv1D	72.8	27.8	
Quad-dir.	73.8	33.1	Conv1D	72.8	28.4	
Oct-dir.	73.5	32.4	Conv2D	73.7	31.7	

(c) Positional Embedding				(d) Concurrency		
Pos. Embed.	IN1K	ADE20K	Concurrency	IN1K	ADE20K	
\times	73.7	31.0	Sequential	73.7	31.7	
\checkmark	73.7	31.7	Parallel	73.0	30.6	

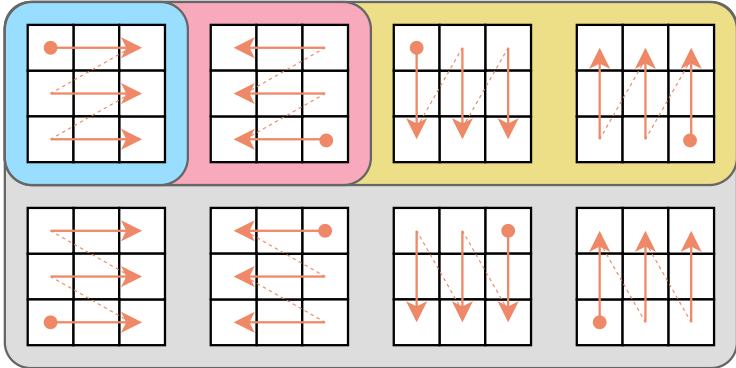


Figure 4: **Uni-directional**, **bi-directional**, **quad-directional** and **oct-directional** traversal paths. Squares represent individual patch tokens. Traversal starts at the circle and goes in direction of the arrow, if no further patches are in a row/column, the traversal continues in the next row/column as indicated by the dashed line.

(a) Traversal Directions Traversing the sequence in at least two directions greatly improves performance due to the non-causal 2D structure of images. Adding column-wise

traversal directions (Quad-dir.) could even further improve semantic segmentation performance. Additionally using 4 instead of 2 starting positions (Oct-dir.) shows no benefit. Note that all variants have the same amount of FLOPS due to sequential application of different directions. Directions are visualized in 4.

We use “Bi-dir.” for our final models due to current technical limitations which would slow down training on more than 2 directions. This limitation comes from the current lack of optimized hardware implementations of the mLSTM (e.g., CUDA kernels) where we instead rely on `torch.compile`, a generic speed optimization method from PyTorch (Paszke et al., 2019), to optimize computations. Our implementation of quad- and oct-directional traversals is not compatible with `torch.compile`, which results in approximately double the runtime. We therefore train all models from Section 3 with “Bi-dir.” only. Note that this is only a technical limitation, not a methodical one and the ablation study suggest that future ViL models could be even better using a quad-directional design.

(b) QK Convolution The mLSTM block design uses a causal 1D convolution to aggregate local context to improve storage/retrieval to/from the cell state \mathbf{C} . This is done by applying a convolution layer to \mathbf{X} before projecting it to \mathbf{Q} with \mathbf{W}_q and \mathbf{K} with \mathbf{W}_k respectively. The convolution is shared for \mathbf{Q} and \mathbf{K} . The causal 1D structure of the convolution from the original mLSTM (Beck et al., 2024) is necessary due to the causal 1D structure of language modeling. However, as images are neither causal nor 1D structures, we replace the causal 1D convolution with a 2D convolution (with kernel size 3). This allows the mLSTM to make better storage/retrieval decisions through the added local context.

(c) Positional Embedding ViTs require positional embedding to tell the model where each patch is located in the image, suffering heavy performance losses if the position is not required (Dosovitskiy et al., 2021; Chu et al., 2023). The mLSTM is an autoregressive model, which makes it optional to add positional embeddings as it can recognize the position of the current patch based on how many patches have been processed. However, the ablation shows that it is nevertheless beneficial to provide this information explicitly as it improves segmentation results without hurting classification performance.

(d) Sequential vs. Parallel Related architectures use a parallel design where a sequence is processed from multiple directions in a single block (Zhu et al., 2024; Duan et al., 2024). We investigate a similar design where we apply both directions in parallel instead of sequentially. To keep parameters and FLOPS constant, we apply the directions akin to parallel transformer blocks (Wang, 2021) while halving the depth.

$$\mathbf{Y} = \mathbf{X} + \text{Block}_\theta(\mathbf{X}) + \text{Flip}(\text{Block}_\phi(\text{Flip}(\mathbf{X}))) \quad (15)$$

4.2 CLASSIFICATION DESIGN

In order to perform classification from a sequence of tokens, it is common to aggregate information from the whole sequence, which is then used as input to a classification head. The most common methods to do this aggregation are (i) adding a learnable [CLS] token to the input sequence or (ii) averaging all patch tokens to produce an [AVG] token. In ViTs, whether to use the [CLS] or [AVG] token is typically a hyperparameter, where both variants achieve comparable performances. On the contrary, other sequence models often require specialized classification designs. For example, Vim (Zhu et al., 2024) requires the [CLS] token to be in the middle of the sequence, suffering heavy performance losses if other classification designs, e.g., an [AVG] token or two [CLS] tokens at start and end of the sequence, are employed.

We explore different classification designs for ViL in Table 5. (a) We choose concatenating the first and last patch as aggregation method due to its strong classification performance. As our final models also perform well in semantic segmentation (see Table 2), we do not retrain models with [AVG] aggregation even though the ablation suggests that this could boost performance even further for segmentation tasks. (b) Adding learnable [CLS] tokens show no benefit. Therefore, we do not use any [CLS] tokens for ViL.

Table 5: Classification design. (a) ViL aggregates classification information well in the first and the last patches (bilateral), leading to good classification performance if the first and last patches are averaged or concatenated. Averaging all patches ([AVG]) or the 4 center patches (Center [AVG]) results in strong segmentation performances but lackluster classification performances. (b) Adding learnable [CLS] tokens to the start and end of the input sequence (Bilateral [CLS]) offers no benefit over simply using the first and the last patch. Incorporating a [CLS] token in the middle of the sequence, akin to Vim (Zhu et al., 2024), does not improve performance. **Default settings**

(a) Patch-based Aggregation			(b) [CLS]-based Aggregation	
Aggregation	IN1K	ADE20K	Aggregation	IN1K
Bilateral Mean	73.0	31.5	Concat Bilateral Patches	73.7
Bilateral Concat	73.7	31.7	Mid [CLS]	71.8
[AVG]	72.6	32.8	Bilateral [CLS]	73.5
Center [AVG]	72.4	32.1	Mid + Bilateral [CLS]	73.0

5 LIMITATIONS AND FUTURE WORK

The biggest limitation of ViL is the current lack of an optimized hardware implementation of the mLSTM, which results in longer runtimes than ViTs, which have multiple optimized hardware implementations (Dao et al., 2022; Dao, 2023). This makes a runtime/throughput analysis of models, a vital metric to judge practicability, difficult as the practical relevance of inefficient implementations is quite low. As a proxy, we report FLOP counts, where ViL is comparable to ViT on low-resolution tasks and far better than ViT on high-resolution tasks due to its linear complexity. While FLOPS are far from an optimal proxy for runtime/throughput, they suggest that ViL can be much faster than ViT on high-resolution tasks once an optimized hardware implementation exists. Note that ViL is already faster than Vim (see Appendix A.1) despite its optimized hardware implementation.

This limitation snowballs in multiple other directions. For example, scaling model size further, tuning hyperparameters, training on larger datasets, exploring self-supervised pre-training or investigating hierarchical architectures are all interesting avenues for future work that are currently quite costly due to the lack of an optimized hardware implementation.

Please note that this is merely a technical limitation, not a methodical one as the mLSTM is heavily parallelizable. However, implementing fast compute kernels in CUDA (NVIDIA et al., 2020) or Triton (Tillet et al., 2019) is highly non-trivial as it requires expert hardware architecture knowledge, advanced implementation skills and potentially multiple development cycles to iron out numerical inaccuracies or instabilities.

However, the results of recent linear attention mechanisms show impressive FLOPS utilization (e.g., Yang et al. (2024)). As the mLSTM can be parallelized with similar techniques it is only a matter of time that the mLSTM achieves a similar FLOPS utilization, which will make the mLSTM faster than transformers once an efficient hardware implementation is available.

Additionally, we made a significant effort to make our architecture as efficient as possible, using the tools that are currently available to us. Notably, our architecture is already much faster (up to 70%) than Vim (Zhu et al., 2024) despite Vim using a custom CUDA kernel, as shown in Appendix A.1. For reference, in language modeling, Mamba is roughly on-par with transformers in terms of speed and 4x faster than the xLSTM (as mentioned in Beck et al. (2024)), again, due to the current lack of efficient hardware implementation of the mLSTM. These considerations further underline the potential of our simple and efficient design for vision applications.

486 6 RELATED WORK

487
488 **Generic Vision Backbones.** The inductive bias of CNNs (Fukushima, 1980; Le-
489 Cun et al., 1998) has demonstrated ground-breaking advancements in computer vi-
490 sion (Krizhevsky et al., 2012) in the early deep learning days. Features of CNNs have
491 been found to learn generic visual features that can be used for a variety of tasks (Donahue
492 et al., 2014). Subsequently, countless works improved various aspects such as architec-
493 tures (Szegedy et al., 2015; He et al., 2016; Huang et al., 2017; Tan & Le, 2019; Liu et al.,
494 2022) or pre-training strategy (Doersch et al., 2015; Noroozi & Favaro, 2016; Zhang et al.,
495 2016; Gidaris et al., 2018; Chen et al., 2020b; Grill et al., 2020).

496 **Sequence Models in Vision.** The introduction of transformers (Vaswani et al., 2017)
497 demonstrated exceptional scalability in language processing, which motivated the vision
498 community to explore transformers also in computer vision (Chen et al., 2020a; Cordonnier
499 et al., 2020) but was applied on pixels or small patches which inhibited large costs due to the
500 quadratic complexity of self-attention. This restriction was alleviated by the seminal work
501 Vision Transformers (ViTs) (Dosovitskiy et al., 2021) by using larger patches to aggregate
502 local information and reduce training costs. Similar to CNNs, lots of work improved on
503 the ViT architecture by refining training procedures (Touvron et al., 2021a;b; 2022b; Caron
504 et al., 2021; Bao et al., 2022; Xie et al., 2022; He et al., 2022). The recent advancement of
505 autoregressive models in language processing (Gu & Dao, 2023; Peng et al., 2023) has also
506 gathered interest in the vision community (Zhu et al., 2024; Duan et al., 2024) due to the
507 linear scaling property which allows applications to high-resolution tasks such as medical
508 imaging (Ma et al., 2024) or video understanding (Li et al., 2024).

509 7 CONCLUSION

510 Motivated by the success of xLSTM in language modeling, we introduced ViL, an adaption
511 of the xLSTM architecture to vision tasks. ViL processes a sequence of patch tokens in
512 alternating fashion. Odd blocks process image patches row-wise from top left to bottom right
513 and even blocks go row-wise from bottom right to top left. Our new architecture outperforms
514 SSM-based vision architectures, other autoregressive vision architectures and also optimized
515 ViT models on ImageNet-1K classification, VTAB-1K transfer classification and ADE20K
516 semantic segmentation. Remarkably, ViL is able to outperform ViT training pipelines,
517 which are the result of years of hyperparameter tuning and transformer improvements.

518 In the future, we see potential in applying ViL when high-resolution images are needed
519 for optimal performance, such as semantic segmentation or medical imaging. In these set-
520 tings, transformers suffer from high computational costs due to the quadratic complexity
521 of self-attention, where the linear complexity of ViL allows compute efficient processing of
522 long sequences. Additionally, improving pre-training schemes (e.g., via self-supervised learn-
523 ing), exploring better hyperparameter settings or investigating hierarchical architectures are
524 promising future directions that could improve ViL even further.
525
526
527
528
529
530
531
532
533
534
535
536
537
538
539

540 REPRODUCIBILITY

541
542 The supplemental material contains the full anonymized codebase used for all experiments
543 in this paper together with the exact hyperparameter configurations that were used for
544 each experiment. Additionally, we provide the hyperparameters for training and evaluation
545 together with additional implementation details for FLOP counting in Appendix Section B.
546

547 ETHICS STATEMENT

548
549 Our work proposes a novel architecture that shows improved FLOPS efficiency compared
550 to previous methods which could greatly reduce energy consumption and carbon emission
551 for future training of large-scale vision or multi-modal models.
552

553 We proposes a foundational change in the form of a novel vision architecture, which can be
554 used for a broad set of applications, inheriting their potential benefits, such as enhancing
555 diagnostic accuracy in healthcare, and challenges, such as the risk of improving generative
556 vision models to generate better deepfakes to propagate misinformation.
557

558 REFERENCES

- 559 Josh Achiam, Steven Adler, Sandhini Agarwal, Lama Ahmad, Ilge Akkaya, Florencia Leoni
560 Aleman, Diogo Almeida, Janko Altenschmidt, Sam Altman, Shyamal Anadkat, et al.
561 Gpt-4 technical report. *arXiv preprint arXiv:2303.08774*, 2023.
562
- 563 Benedikt Alkin, Andreas Fürst, Simon Schmid, Lukas Gruber, Markus Holzleitner, and
564 Johannes Brandstetter. Universal physics transformers. *arXiv preprint arXiv:2402.12365*,
565 2024a.
566
- 567 Benedikt Alkin, Lukas Miklautz, Sepp Hochreiter, and Johannes Brandstetter. Mim-refiner:
568 A contrastive learning boost from intermediate pre-trained representations. *arXiv preprint*
569 *arXiv:2402.10093*, 2024b.
- 570 Hangbo Bao, Li Dong, Songhao Piao, and Furu Wei. Beit: BERT pre-training of image
571 transformers. In *The Tenth International Conference on Learning Representations, ICLR*
572 *2022, Virtual Event, April 25-29, 2022*. OpenReview.net, 2022.
573
- 574 Maximilian Beck, Korbinian Pöppel, Markus Spanring, Andreas Auer, Oleksandra Prud-
575 nikova, Michael Kopp, Günter Klambauer, Johannes Brandstetter, and Sepp Hochreiter.
576 xlstm: Extended long short-term memory, 2024.
- 577 Kaifeng Bi, Lingxi Xie, Hengheng Zhang, Xin Chen, Xiaotao Gu, and Qi Tian. Accurate
578 medium-range global weather forecasting with 3d neural networks. *Nature*, 619(7970):
579 533–538, 2023.
580
- 581 Cristian Bodnar, Wessel P Bruinsma, Ana Lucic, Megan Stanley, Johannes Brandstetter,
582 Patrick Garvan, Maik Riechert, Jonathan Weyn, Haiyu Dong, Anna Vaughan, et al.
583 Aurora: A foundation model of the atmosphere. *arXiv preprint arXiv:2405.13063*, 2024.
584
- 585 Kaj Bostrom and Greg Durrett. Byte pair encoding is suboptimal for language model
586 pretraining. *arXiv preprint arXiv:2004.03720*, 2020.
- 587 Mathilde Caron, Hugo Touvron, Ishan Misra, Hervé Jégou, Julien Mairal, Piotr Bojanowski,
588 and Armand Joulin. Emerging properties in self-supervised vision transformers. In *2021*
589 *IEEE/CVF International Conference on Computer Vision, ICCV 2021, Montreal, QC,*
590 *Canada, October 10-17, 2021*, pp. 9630–9640. IEEE, 2021.
591
- 592 Jieneng Chen, Yongyi Lu, Qihang Yu, Xiangde Luo, Ehsan Adeli, Yan Wang, Le Lu, Alan L.
593 Yuille, and Yuyin Zhou. Transunet: Transformers make strong encoders for medical image
segmentation. *CoRR*, abs/2102.04306, 2021.

- 594 Mark Chen, Alec Radford, Rewon Child, Jeffrey Wu, Heewoo Jun, David Luan, and Ilya
595 Sutskever. Generative pretraining from pixels. In *Proceedings of the 37th International*
596 *Conference on Machine Learning, ICML 2020, 13-18 July 2020, Virtual Event*, volume
597 119 of *Proceedings of Machine Learning Research*, pp. 1691–1703. PMLR, 2020a.
- 598
599 Ting Chen, Simon Kornblith, Mohammad Norouzi, and Geoffrey E. Hinton. A simple
600 framework for contrastive learning of visual representations. In *Proceedings of the 37th*
601 *International Conference on Machine Learning, ICML 2020, 13-18 July 2020, Virtual*
602 *Event*, volume 119 of *Proceedings of Machine Learning Research*, pp. 1597–1607. PMLR,
603 2020b.
- 604 Bowen Cheng, Ishan Misra, Alexander G. Schwing, Alexander Kirillov, and Rohit Girdhar.
605 Masked-attention mask transformer for universal image segmentation. In *IEEE/CVF*
606 *Conference on Computer Vision and Pattern Recognition, CVPR 2022, New Orleans,*
607 *LA, USA, June 18-24, 2022*, pp. 1280–1289. IEEE, 2022.
- 608
609 Gong Cheng, Junwei Han, and Xiaoqiang Lu. Remote sensing image scene classification:
610 Benchmark and state of the art. *Proc. IEEE*, 105(10):1865–1883, 2017.
- 611 Xiangxiang Chu, Zhi Tian, Bo Zhang, Xinlong Wang, and Chunhua Shen. Conditional
612 positional encodings for vision transformers. In *ICLR. OpenReview.net*, 2023.
- 613
614 Jean-Baptiste Cordonnier, Andreas Loukas, and Martin Jaggi. On the relationship between
615 self-attention and convolutional layers. In *8th International Conference on Learning Rep-*
616 *resentations, ICLR 2020, Addis Ababa, Ethiopia, April 26-30, 2020*. OpenReview.net,
617 2020. URL <https://openreview.net/forum?id=HJ1nC1rKPB>.
- 618
619 Tri Dao. Flashattention-2: Faster attention with better parallelism and work partitioning.
620 *CoRR*, abs/2307.08691, 2023.
- 621
622 Tri Dao, Daniel Y. Fu, Stefano Ermon, Atri Rudra, and Christopher Ré. Flashattention:
623 Fast and memory-efficient exact attention with io-awareness. In *NeurIPS*, 2022.
- 624
625 Jia Deng, Wei Dong, Richard Socher, Li-Jia Li, Kai Li, and Li Fei-Fei. Imagenet: A
626 large-scale hierarchical image database. In *2009 IEEE Computer Society Conference*
627 *on Computer Vision and Pattern Recognition (CVPR 2009), 20-25 June 2009, Miami,*
Florida, USA, pp. 248–255. IEEE Computer Society, 2009.
- 628
629 Carl Doersch, Abhinav Gupta, and Alexei A. Efros. Unsupervised visual representation
630 learning by context prediction. In *2015 IEEE International Conference on Computer Vi-*
631 *sion, ICCV 2015, Santiago, Chile, December 7-13, 2015*, pp. 1422–1430. IEEE Computer
632 Society, 2015.
- 633
634 Jeff Donahue, Yangqing Jia, Oriol Vinyals, Judy Hoffman, Ning Zhang, Eric Tzeng, and
635 Trevor Darrell. Decaf: A deep convolutional activation feature for generic visual recog-
636 nition. In *Proceedings of the 31th International Conference on Machine Learning, ICML*
637 *2014, Beijing, China, 21-26 June 2014*, volume 32 of *JMLR Workshop and Conference*
Proceedings, pp. 647–655. JMLR.org, 2014.
- 638
639 Alexey Dosovitskiy, Lucas Beyer, Alexander Kolesnikov, Dirk Weissenborn, Xiaohua Zhai,
640 Thomas Unterthiner, Mostafa Dehghani, Matthias Minderer, Georg Heigold, Sylvain
641 Gelly, Jakob Uszkoreit, and Neil Houlsby. An image is worth 16x16 words: Transformers
642 for image recognition at scale. In *9th International Conference on Learning Representa-*
tions, ICLR 2021, Virtual Event, Austria, May 3-7, 2021. OpenReview.net, 2021.
- 643
644 Yuchen Duan, Weiyun Wang, Zhe Chen, Xizhou Zhu, Lewei Lu, Tong Lu, Yu Qiao, Hong-
645 sheng Li, Jifeng Dai, and Wenhui Wang. Vision-rwkv: Efficient and scalable visual per-
646 ception with rwkv-like architectures. *CoRR*, abs/2403.02308, 2024.
- 647
Li Fei-Fei, Robert Fergus, and Pietro Perona. One-shot learning of object categories. *IEEE*
transactions on pattern analysis and machine intelligence, 28(4):594–611, 2006.

- 648 Kuniyiko Fukushima. Neocognitron: A self-organizing neural network model for a mecha-
649 nism of pattern recognition unaffected by shift in position. *Biological cybernetics*, 36(4):
650 193–202, 1980.
- 651 Andreas Geiger, Philip Lenz, Christoph Stiller, and Raquel Urtasun. Vision meets robotics:
652 The KITTI dataset. *Int. J. Robotics Res.*, 32(11):1231–1237, 2013.
- 653
654 Spyros Gidaris, Praveer Singh, and Nikos Komodakis. Unsupervised representation learn-
655 ing by predicting image rotations. In *6th International Conference on Learning Repre-*
656 *sentations, ICLR 2018, Vancouver, BC, Canada, April 30 - May 3, 2018, Conference*
657 *Track Proceedings*. OpenReview.net, 2018. URL [https://openreview.net/forum?id=](https://openreview.net/forum?id=S1v4N210-)
658 [S1v4N210-](https://openreview.net/forum?id=S1v4N210-).
- 659 Jean-Bastien Grill, Florian Strub, Florent Althé, Corentin Tallec, Pierre H. Richemond,
660 Elena Buchatskaya, Carl Doersch, Bernardo Ávila Pires, Zhaohan Guo, Moham-
661 mad Gheshlaghi Azar, Bilal Piot, Koray Kavukcuoglu, Rémi Munos, and Michal Valko.
662 Bootstrap your own latent - A new approach to self-supervised learning. In Hugo
663 Larochelle, Marc’Aurelio Ranzato, Raia Hadsell, Maria-Florina Balcan, and Hsuan-Tien
664 Lin (eds.), *Advances in Neural Information Processing Systems 33: Annual Conference*
665 *on Neural Information Processing Systems 2020, NeurIPS 2020, December 6-12, 2020,*
666 *virtual*, 2020.
- 667
668 A. Gu, K. Goel, and C. Ré. Efficiently modeling long sequences with structured state spaces.
669 *ArXiv*, 2111.00396, 2021.
- 670 Albert Gu and Tri Dao. Mamba: Linear-time sequence modeling with selective state spaces.
671 *CoRR*, abs/2312.00752, 2023.
- 672
673 A. Gupta, A. Gu, and J. Berant. Diagonal state spaces are as effective as structured state
674 spaces. *ArXiv*, 2203.14343, 2022.
- 675 Ali Hatamizadeh, Yucheng Tang, Vishwesh Nath, Dong Yang, Andriy Myronenko, Ben-
676 nett A. Landman, Holger R. Roth, and Daguang Xu. UNETR: transformers for 3d medi-
677 cal image segmentation. In *IEEE/CVF Winter Conference on Applications of Computer*
678 *Vision, WACV 2022, Waikoloa, HI, USA, January 3-8, 2022*, pp. 1748–1758. IEEE, 2022.
- 679
680 Kaiming He, Xiangyu Zhang, Shaoqing Ren, and Jian Sun. Deep residual learning for image
681 recognition. In *2016 IEEE Conference on Computer Vision and Pattern Recognition,*
682 *CVPR 2016, Las Vegas, NV, USA, June 27-30, 2016*, pp. 770–778. IEEE Computer
683 Society, 2016.
- 684
685 Kaiming He, Xinlei Chen, Saining Xie, Yanghao Li, Piotr Dollár, and Ross B. Girshick.
686 Masked autoencoders are scalable vision learners. In *Proceedings of the IEEE/CVF Con-*
687 *ference on Computer Vision and Pattern Recognition, CVPR 2022*, pp. 15979–15988,
2022.
- 688
689 Patrick Helber, Benjamin Bischke, Andreas Dengel, and Damian Borth. Eurosat: A novel
690 dataset and deep learning benchmark for land use and land cover classification. *IEEE J.*
691 *Sel. Top. Appl. Earth Obs. Remote. Sens.*, 12(7):2217–2226, 2019.
- 692
693 Dan Hendrycks and Thomas G. Dietterich. Benchmarking neural network robustness to
694 common corruptions and perturbations. In *ICLR (Poster)*. OpenReview.net, 2019.
- 695
696 Dan Hendrycks, Steven Basart, Norman Mu, Saurav Kadavath, Frank Wang, Evan Dorundo,
697 Rahul Desai, Tyler Zhu, Samyak Parajuli, Mike Guo, Dawn Song, Jacob Steinhardt, and
Justin Gilmer. The many faces of robustness: A critical analysis of out-of-distribution
generalization. *ICCV*, 2021a.
- 698
699 Dan Hendrycks, Kevin Zhao, Steven Basart, Jacob Steinhardt, and Dawn Song. Natural
700 adversarial examples. *CVPR*, 2021b.
- 701
Sepp Hochreiter and Jürgen Schmidhuber. Long short-term memory. *Neural computation*,
9(8):1735–1780, 1997.

- 702 Gao Huang, Yu Sun, Zhuang Liu, Daniel Sedra, and Kilian Q. Weinberger. Deep net-
703 works with stochastic depth. In Bastian Leibe, Jiri Matas, Nicu Sebe, and Max Welling
704 (eds.), *Computer Vision - ECCV 2016 - 14th European Conference, Amsterdam, The*
705 *Netherlands, October 11-14, 2016, Proceedings, Part IV*, volume 9908 of *Lecture Notes in*
706 *Computer Science*, pp. 646–661. Springer, 2016.
- 707 Gao Huang, Zhuang Liu, Laurens van der Maaten, and Kilian Q. Weinberger. Densely
708 connected convolutional networks. In *2017 IEEE Conference on Computer Vision and*
709 *Pattern Recognition, CVPR 2017, Honolulu, HI, USA, July 21-26, 2017*, pp. 2261–2269.
710 IEEE Computer Society, 2017.
- 711 Justin Johnson, Bharath Hariharan, Laurens van der Maaten, Li Fei-Fei, C. Lawrence Zit-
712 nick, and Ross B. Girshick. CLEVR: A diagnostic dataset for compositional language and
713 elementary visual reasoning. In *2017 IEEE Conference on Computer Vision and Pattern*
714 *Recognition, CVPR 2017, Honolulu, HI, USA, July 21-26, 2017*, pp. 1988–1997. IEEE
715 Computer Society, 2017.
- 716 Kaggle and EyePacs. Kaggle diabetic retinopathy detection, July 2015.
- 717 Alexander Kirillov, Eric Mintun, Nikhila Ravi, Hanzi Mao, Chloé Rolland, Laura Gustafson,
718 Tete Xiao, Spencer Whitehead, Alexander C. Berg, Wan-Yen Lo, Piotr Dollár, and Ross B.
719 Girshick. Segment anything. In *ICCV*, pp. 3992–4003. IEEE, 2023.
- 720 Alex Krizhevsky. Learning multiple layers of features from tiny images. 2009.
- 721 Alex Krizhevsky, Ilya Sutskever, and Geoffrey E. Hinton. Imagenet classification with deep
722 convolutional neural networks. In Peter L. Bartlett, Fernando C. N. Pereira, Christopher
723 J. C. Burges, Léon Bottou, and Kilian Q. Weinberger (eds.), *Advances in Neural Informa-*
724 *tion Processing Systems 25: 26th Annual Conference on Neural Information Processing*
725 *Systems 2012. Proceedings of a meeting held December 3-6, 2012, Lake Tahoe, Nevada,*
726 *United States*, pp. 1106–1114, 2012.
- 727 Yann LeCun, Léon Bottou, Yoshua Bengio, and Patrick Haffner. Gradient-based learning
728 applied to document recognition. *Proc. IEEE*, 86(11):2278–2324, 1998.
- 729 Kunchang Li, Xinhao Li, Yi Wang, Yinan He, Yali Wang, Limin Wang, and Yu Qiao. Video-
730 mamba: State space model for efficient video understanding. *CoRR*, abs/2403.06977,
731 2024.
- 732 Yue Liu, Yunjie Tian, Yuzhong Zhao, Hongtian Yu, Lingxi Xie, Yaowei Wang, Qixiang Ye,
733 and Yunfan Liu. Vmamba: Visual state space model. *CoRR*, abs/2401.10166, 2024.
- 734 Zhuang Liu, Hanzi Mao, Chao-Yuan Wu, Christoph Feichtenhofer, Trevor Darrell, and
735 Saining Xie. A convnet for the 2020s. In *IEEE/CVF Conference on Computer Vision*
736 *and Pattern Recognition, CVPR 2022, New Orleans, LA, USA, June 18-24, 2022*, pp.
737 11966–11976. IEEE, 2022.
- 738 Jun Ma, Feifei Li, and Bo Wang. U-mamba: Enhancing long-range dependency for biomed-
739 ical image segmentation. *CoRR*, abs/2401.04722, 2024.
- 740 Tung Nguyen, Johannes Brandstetter, Ashish Kapoor, Jayesh K Gupta, and Aditya Grover.
741 Climax: A foundation model for weather and climate. *arXiv preprint arXiv:2301.10343*,
742 2023.
- 743 Mehdi Noroozi and Paolo Favaro. Unsupervised learning of visual representations by solving
744 jigsaw puzzles. In Bastian Leibe, Jiri Matas, Nicu Sebe, and Max Welling (eds.), *Computer*
745 *Vision - ECCV 2016 - 14th European Conference, Amsterdam, The Netherlands, October*
746 *11-14, 2016, Proceedings, Part VI*, volume 9910 of *Lecture Notes in Computer Science*,
747 pp. 69–84. Springer, 2016.
- 748 NVIDIA, Péter Vingelmann, and Frank H.P. Fitzek. Cuda, release: 10.2.89, 2020. URL
749 <https://developer.nvidia.com/cuda-toolkit>.

- 756 Maxime Oquab, Timothée Darcet, Théo Moutakanni, Huy Vo, Marc Szafraniec, Vasil Khali-
757 dov, Pierre Fernandez, Daniel Haziza, Francisco Massa, Alaaeldin El-Nouby, Mahmoud
758 Assran, Nicolas Ballas, Wojciech Galuba, Russell Howes, Po-Yao Huang, Shang-Wen Li,
759 Ishan Misra, Michael G. Rabbat, Vasu Sharma, Gabriel Synnaeve, Hu Xu, Hervé Jégou,
760 Julien Mairal, Patrick Labatut, Armand Joulin, and Piotr Bojanowski. Dinov2: Learning
761 robust visual features without supervision. *CoRR*, abs/2304.07193, 2023.
- 762 Adam Paszke, Sam Gross, Francisco Massa, Adam Lerer, James Bradbury, Gregory Chanan,
763 Trevor Killeen, Zeming Lin, Natalia Gimelshein, Luca Antiga, Alban Desmaison, Andreas
764 Köpf, Edward Z. Yang, Zachary DeVito, Martin Raison, Alykhan Tejani, Sasank Chil-
765 amkurthy, Benoit Steiner, Lu Fang, Junjie Bai, and Soumith Chintala. Pytorch: An
766 imperative style, high-performance deep learning library. In *NeurIPS*, pp. 8024–8035,
767 2019.
- 768 William Peebles and Saining Xie. Scalable diffusion models with transformers. In
769 *IEEE/CVF International Conference on Computer Vision, ICCV 2023, Paris, France,*
770 *October 1-6, 2023*, pp. 4172–4182. IEEE, 2023.
- 771 Bo Peng, Eric Alcaide, Quentin Anthony, Alon Albalak, Samuel Arcadinho, Stella Bider-
772 man, Huanqi Cao, Xin Cheng, Michael Chung, Leon Derczynski, Xingjian Du, Matteo
773 Grella, Kranthi Kiran GV, Xuzheng He, Haowen Hou, Przemyslaw Kazienko, Jan Kocon,
774 Jiaming Kong, Bartłomiej Koptyra, Hayden Lau, Jiaju Lin, Krishna Sri Ipsit Mantri,
775 Ferdinand Mom, Atsushi Saito, Guangyu Song, Xiangru Tang, Johan S. Wind, Stanislaw
776 Wozniak, Zhenyuan Zhang, Qinghua Zhou, Jian Zhu, and Rui-Jie Zhu. RWKV: reinvent-
777 ing rnns for the transformer era. In *EMNLP (Findings)*, pp. 14048–14077. Association
778 for Computational Linguistics, 2023.
- 779 Mannat Singh, Quentin Duval, Kalyan Vasudev Alwala, Haoqi Fan, Vaibhav Aggarwal,
780 Aaron Adcock, Armand Joulin, Piotr Dollár, Christoph Feichtenhofer, Ross B. Girshick,
781 Rohit Girdhar, and Ishan Misra. The effectiveness of MAE pre-pretraining for billion-scale
782 pretraining. *CoRR*, abs/2303.13496, 2023.
- 783 Christian Szegedy, Wei Liu, Yangqing Jia, Pierre Sermanet, Scott E. Reed, Dragomir
784 Anguelov, Dumitru Erhan, Vincent Vanhoucke, and Andrew Rabinovich. Going deeper
785 with convolutions. In *IEEE Conference on Computer Vision and Pattern Recognition,*
786 *CVPR 2015, Boston, MA, USA, June 7-12, 2015*, pp. 1–9. IEEE Computer Society, 2015.
- 787 Mingxing Tan and Quoc V. Le. Efficientnet: Rethinking model scaling for convolutional
788 neural networks. In Kamalika Chaudhuri and Ruslan Salakhutdinov (eds.), *Proceedings*
789 *of the 36th International Conference on Machine Learning, ICML 2019, 9-15 June 2019,*
790 *Long Beach, California, USA*, volume 97 of *Proceedings of Machine Learning Research*,
791 pp. 6105–6114. PMLR, 2019.
- 792 Gemini Team, Rohan Anil, Sebastian Borgeaud, Yonghui Wu, Jean-Baptiste Alayrac, Jiahui
793 Yu, Radu Soricut, Johan Schalkwyk, Andrew M Dai, Anja Hauth, et al. Gemini: a family
794 of highly capable multimodal models. *arXiv preprint arXiv:2312.11805*, 2023.
- 795 Philippe Tillet, Hsiang-Tsung Kung, and David D. Cox. Triton: an intermediate lan-
796 guage and compiler for tiled neural network computations. In Tim Mattson, Abdullah
797 Muzahid, and Armando Solar-Lezama (eds.), *Proceedings of the 3rd ACM SIGPLAN In-*
798 *ternational Workshop on Machine Learning and Programming Languages, MAPL@PLDI*
799 *2019, Phoenix, AZ, USA, June 22, 2019*, pp. 10–19. ACM, 2019.
- 800 Hugo Touvron, Matthieu Cord, Matthijs Douze, Francisco Massa, Alexandre Sablayrolles,
801 and Hervé Jégou. Training data-efficient image transformers & distillation through atten-
802 tion. In *ICML*, volume 139 of *Proceedings of Machine Learning Research*, pp. 10347–10357.
803 PMLR, 2021a.
- 804 Hugo Touvron, Matthieu Cord, Alexandre Sablayrolles, Gabriel Synnaeve, and Hervé Jégou.
805 Going deeper with image transformers. In *ICCV*, pp. 32–42. IEEE, 2021b.

- 810 Hugo Touvron, Matthieu Cord, Alaaeldin El-Nouby, Jakob Verbeek, and Hervé Jégou. Three
811 things everyone should know about vision transformers. In *ECCV (24)*, volume 13684 of
812 *Lecture Notes in Computer Science*, pp. 497–515. Springer, 2022a.
- 813
- 814 Hugo Touvron, Matthieu Cord, and Hervé Jégou. Deit III: revenge of the vit. In *ECCV*
815 *(24)*, volume 13684 of *Lecture Notes in Computer Science*, pp. 516–533. Springer, 2022b.
- 816
- 817 Hugo Touvron, Matthieu Cord, Maxime Oquab, Piotr Bojanowski, Jakob Verbeek, and
818 Hervé Jégou. Co-training 2l submodels for visual recognition. In *IEEE/CVF Conference*
819 *on Computer Vision and Pattern Recognition, CVPR 2023, Vancouver, BC, Canada,*
820 *June 17-24, 2023*, pp. 11701–11710. IEEE, 2023.
- 821 Jeya Maria Jose Valanarasu, Poojan Oza, Ilker Hacihaliloglu, and Vishal M. Patel. Medical
822 transformer: Gated axial-attention for medical image segmentation. In Marleen de Brui-
823 jne, Philippe C. Cattin, Stéphane Cotin, Nicolas Padoy, Stefanie Speidel, Yefeng Zheng,
824 and Caroline Essert (eds.), *Medical Image Computing and Computer Assisted Intervention - MICCAI 2021 - 24th International Conference, Strasbourg, France, September 27 -*
825 *October 1, 2021, Proceedings, Part I*, volume 12901 of *Lecture Notes in Computer Science*,
826 pp. 36–46. Springer, 2021.
- 827
- 828 Ashish Vaswani, Noam Shazeer, Niki Parmar, Jakob Uszkoreit, Llion Jones, Aidan N Gomez,
829 Lukasz Kaiser, and Illia Polosukhin. Attention is all you need. *Advances in neural infor-*
830 *mation processing systems*, 30, 2017.
- 831
- 832 Bastiaan S. Veeling, Jasper Linmans, Jim Winkens, Taco Cohen, and Max Welling. Rota-
833 tion equivariant cnns for digital pathology. In Alejandro F. Frangi, Julia A. Schnabel,
834 Christos Davatzikos, Carlos Alberola-López, and Gabor Fichtinger (eds.), *Medical Im-*
835 *age Computing and Computer Assisted Intervention - MICCAI 2018 - 21st International*
836 *Conference, Granada, Spain, September 16-20, 2018, Proceedings, Part II*, volume 11071
837 of *Lecture Notes in Computer Science*, pp. 210–218. Springer, 2018.
- 838
- 839 Ben Wang. Mesh-Transformer-JAX: Model-Parallel Implementation of Transformer Lan-
840 guage Model with JAX. <https://github.com/kingoflolz/mesh-transformer-jax>,
841 2021.
- 842
- 843 Feng Wang, Jiahao Wang, Sucheng Ren, Guoyizhe Wei, Jieru Mei, Wei Shao, Yuyin Zhou,
844 Alan Yuille, and Cihang Xie. Mamba-r: Vision mamba also needs registers. *arXiv preprint*
845 *arXiv:2405.14858*, 2024.
- 846
- 847 Haohan Wang, Songwei Ge, Zachary Lipton, and Eric P Xing. Learning robust global
848 representations by penalizing local predictive power. In *Advances in Neural Information*
Processing Systems, pp. 10506–10518, 2019.
- 849
- 850 Tete Xiao, Yingcheng Liu, Bolei Zhou, Yuning Jiang, and Jian Sun. Unified perceptual
851 parsing for scene understanding. In Vittorio Ferrari, Martial Hebert, Cristian Sminchis-
852 escu, and Yair Weiss (eds.), *Computer Vision - ECCV 2018 - 15th European Conference,*
853 *Munich, Germany, September 8-14, 2018, Proceedings, Part V*, volume 11209 of *Lecture*
Notes in Computer Science, pp. 432–448. Springer, 2018.
- 854
- 855 Zhenda Xie, Zheng Zhang, Yue Cao, Yutong Lin, Jianmin Bao, Zhuliang Yao, Qi Dai,
856 and Han Hu. Simmim: a simple framework for masked image modeling. In *IEEE/CVF*
857 *Conference on Computer Vision and Pattern Recognition, CVPR 2022, New Orleans,*
858 *LA, USA, June 18-24, 2022*, pp. 9643–9653. IEEE, 2022.
- 859
- 860 Hanwen Xu, Naoto Usuyama, Jaspreet Bagga, Sheng Zhang, Rajesh Rao, Tristan Naumann,
861 Cliff Wong, Zelalem Gero, Javier González, Yu Gu, et al. A whole-slide foundation model
862 for digital pathology from real-world data. *Nature*, pp. 1–8, 2024.
- 863
- 864 Songlin Yang, Bailin Wang, Yikang Shen, Rameswar Panda, and Yoon Kim. Gated linear
attention transformers with hardware-efficient training. In *ICML*. OpenReview.net, 2024.

864 Xiaohua Zhai, Joan Puigcerver, Alexander Kolesnikov, Pierre Ruysen, Carlos Riquelme,
865 Mario Lucic, Josip Djolonga, Andre Susano Pinto, Maxim Neumann, Alexey Dosovitskiy,
866 et al. A large-scale study of representation learning with the visual task adaptation
867 benchmark. *arXiv preprint arXiv:1910.04867*, 2019.

868 Richard Zhang, Phillip Isola, and Alexei A. Efros. Colorful image colorization. In Bastian
869 Leibe, Jiri Matas, Nicu Sebe, and Max Welling (eds.), *Computer Vision - ECCV 2016 -*
870 *14th European Conference, Amsterdam, The Netherlands, October 11-14, 2016, Proceed-*
871 *ings, Part III*, volume 9907 of *Lecture Notes in Computer Science*, pp. 649–666. Springer,
872 2016.

873 Bolei Zhou, Hang Zhao, Xavier Puig, Tete Xiao, Sanja Fidler, Adela Barriuso, and Antonio
874 Torralba. Semantic understanding of scenes through the ADE20K dataset. *Int. J. Comput.*
875 *Vis.*, 127(3):302–321, 2019.

876 Lianghui Zhu, Bencheng Liao, Qian Zhang, Xinlong Wang, Wenyu Liu, and Xinggang
877 Wang. Vision mamba: Efficient visual representation learning with bidirectional state
878 space model. *CoRR*, abs/2401.09417, 2024.

879
880
881
882
883
884
885
886
887
888
889
890
891
892
893
894
895
896
897
898
899
900
901
902
903
904
905
906
907
908
909
910
911
912
913
914
915
916
917

A EXTENDED RESULTS

A.1 RUNTIME COMPARISON OF ViL VS ViM

We compare the runtime to train ViL and Vim (Zhu et al., 2024) for 10 ImageNet-1K epochs in Table 6. We follow the scaling procedure of ViTs, using 192 (T), 384 (S), 768 (B), 1024 (L) as hidden dimension where the (L)arge scale doubles the number of blocks.

Table 6: Runtime comparisons between Vim (Zhu et al., 2024) and ViL. ViL is up to 69% faster despite the current lack of a optimized hardware implementation. As mLSTM (and ViL) can be parallelized analogous to FlashAttention (Dao et al., 2022; Dao, 2023) via custom hardware optimizations, ViL will become even faster in the future. Runtimes denote the training time for 10 ImageNet-1K epochs and are extrapolated from short benchmark runs on a single A100-80GB-PCIe using float16 precision and 224x224 images.

Model	Optimization	(T)iny	(S)mall	(B)ase	(L)arge
Vim (Zhu et al., 2024)	custom CUDA kernel	7.3h	14.0h	28.2h	76.4h
ViL	<code>torch.compile</code>	5.0h	8.7h	16.6h	45.1h
Speedup of ViL compared to Vim		45%	61%	69%	69%

A.2 IMPACT OF LONGER TRAINING

We investigate the impact of training for a longer duration in Table 7.

Table 7: Performance comparison of tiny models trained for 400 and 800 epochs. ADE20K mIoU uses single-scale evaluation. All settings follow the ones used in the main paper.

Model	Epochs	IN-1K ACC	VTAB-1K	ADE20K mIoU
DeiT-III-T	400	75.6	67.0	39.1
DeiT-III-T	800	76.2	67.1	39.8
ViL-T	400	77.2	67.8	40.9
ViL-T	800	78.3	68.3	41.2

A.3 VTAB-1K INDIVIDUAL DATASET RESULTS

Table 8 presents accuracies for each individual dataset of the VTAB-1K benchmark.

Table 8: Results on all datasets of the VTAB-1K (Zhai et al., 2019) benchmark.

	Natural						Specialized				Structured								
	Cifar100	Caltech101	DTD	Flower102	Pets	SVHN	Sun397	Camelyon	EuroSAT	Resisc45	Retinopathy	Clevr-Count	Clevr-Dist	DMLab	KITTI-Dist	dSpr-Loc	dSpr-Ori	sNORB-Azim	sNORB-Ele
DeiT-T	47.7	86.4	63.7	85.6	87.0	78.4	35.3	83.0	93.4	80.9	70.7	71.7	60.3	43.1	78.5	67.9	41.6	30.6	32.7
DeiT-III-T	52.3	90.1	62.7	88.8	87.5	83.7	37.9	83.2	93.1	81.1	72.9	76.6	60.8	44.9	79.1	67.5	48.1	31.0	33.3
Vim-T	46.7	86.3	60.7	84.0	88.8	76.1	33.7	82.2	92.9	75.2	72.6	59.8	49.9	39.3	78.2	51.2	43.9	26.9	27.2
ViL-T	54.2	90.2	67.4	90.7	89.9	81.6	41.1	83.4	94.2	82.7	73.1	80.7	61.8	49.4	81.3	57.8	51.8	31.4	34.8
DeiT-S	57.0	88.9	68.2	90.9	90.8	75.4	42.1	83.3	94.0	83.8	74.0	74.6	58.3	45.6	78.2	61.9	47.9	27.1	31.9
DeiT-III-S	58.8	88.6	67.5	90.9	91.7	84.4	43.3	84.4	92.6	82.5	73.5	76.5	57.9	46.2	78.9	58.3	49.7	23.7	27.5
Vim-S	53.0	87.2	64.1	86.8	90.3	65.8	39.7	82.4	93.4	78.0	73.1	63.1	53.2	42.3	78.2	54.1	47.6	27.1	29.3
ViL-S	61.4	89.6	69.2	92.8	91.7	78.7	43.8	85.5	93.9	84.4	73.5	84.0	63.4	51.3	83.3	61.0	55.4	32.4	35.5
DeiT-B	61.8	89.8	67.5	93.7	92.6	84.4	45.6	85.3	95.1	86.3	74.2	77.7	59.9	47.2	81.7	61.7	51.4	30.0	36.2
DeiT-III-B	62.9	89.6	69.6	93.7	93.2	87.0	47.1	85.8	94.1	85.6	73.7	80.5	61.4	48.4	80.9	64.4	55.1	30.2	31.8
ViL-B	64.3	90.0	71.1	93.4	91.4	79.6	46.6	84.7	94.3	85.4	74.4	83.7	62.1	52.7	81.0	63.1	57.6	32.6	39.9

A.4 ROBUSTNESS AND DOMAIN GENERALIZATION

Table 9 presents robustness and OOD evaluations of ImageNet-1K pre-trained classifiers.

Table 9: Robustness and OOD evaluations on ImageNet-C(orrupction) (Hendrycks & Dietterich, 2019), ImageNet-A(dversarial) (Hendrycks et al., 2021b), ImageNet-R(endition) (Hendrycks et al., 2021a) and ImageNet-Sketch (Wang et al., 2019).. For ImageNet-C, we report the mean corruption error (Hendrycks & Dietterich, 2019) with AlexNet (Krizhevsky et al., 2012) as baseline.

Model	IN-C (\downarrow)	IN-A (\uparrow)	IN-R (\uparrow)	Sketch (\uparrow)	Validation (\uparrow)
DeiT-T	69.7	7.6	32.7	19.9	72.2
DeiT-III-T	65.0	11.7	39.4	27.4	76.2
Vim-T	61.8	9.6	38.8	26.9	76.1
ViL-T	59.6	15.2	42.2	30.0	78.3
DeiT-S	54.4	19.6	41.9	29.1	79.8
DeiT-III-S	50.1	23.2	46.6	35.4	81.4
Vim-S	51.5	19.7	44.8	32.5	80.5
ViL-S	50.6	23.8	47.9	35.2	81.5
DeiT-B	48.6	27.9	44.6	32.0	81.8
DeiT-III-B	42.7	36.5	54.1	41.1	83.8
ViL-B	45.3	30.9	51.9	39.0	82.4

B IMPLEMENTATION DETAILS

B.1 HARDWARE

We train models on servers with either 8xA100 or 4xA100 nodes.

We estimate the total number of A100 GPU-hours used for this project to be 38K hours. This estimate includes initial exploration, method development, analysis and evaluations.

B.2 FLOPS CALCULATION

We use the `fvcore`¹ library to count FLOPS and report FLOPS of the mLSTM chunkwise form as described in Section 2.2. For the parallel parts, we report FLOPS for a complexity of $\mathcal{O}((\frac{S}{2} + 1)Sd)$ because the upper triangular entries of the \mathbf{QK} matrix do not need to be calculated due to the causal structure. We justify this by the fact that FlashAttention-2 (Dao, 2023) is approximately 1.7x faster with a causal mask than without. Therefore, an optimized hardware implementation of the mLSTM could also omit the calculation of the upper triangular part of \mathbf{QK} .

As Vim (Zhu et al., 2024) does not report FLOPS and their model makes use of CUDA kernels (which are not counted as FLOPS by `fvcore`), we replace all calls to CUDA kernels with their reference PyTorch implementation and count the FLOPS with `fvcore`.

For the total pre-training compute in Figure 3, we consider an efficient implementation of stochastic depth (Huang et al., 2016; Touvron et al., 2023) which omits the calculation of a dropped block instead of masking it. Therefore, we change the implementation of ViT (Dosovitskiy et al., 2021) to use our efficient stochastic depth implementation. Vim does not use stochastic depth for training as they only train tiny and small models.

¹<https://github.com/facebookresearch/fvcore>

1026 B.3 ViL HYPERPARAMETERS

1027 Table 10 shows detailed hyperparameters used to train ViL models.

1028 Table 10: Hyperparameters for training ViL on ImageNet-1K, inspired by DeiT-III (Touvron
1029 et al., 2022b). We follow the best setting from DeiT-III (Touvron et al., 2022b) and pre-train
1030 on 192 resolution followed by a short fine-tuning on 224 resolution (indicated by \rightarrow).
1031
1032

Parameter	Value
Epochs	800 (T), 400 (S/B) \rightarrow 20 (T, S), 5 (B)
Batch size	2048 \rightarrow 1024
Model	
Patch size	16x16
Latent dimension	192 (T), 384 (S), 768 (B)
Depth	24
Pooling	Bilateral Concat
Stochastic depth	
Peak rate	0 (T), 0.05 (S), 0.2 (B)
Layer-wise Decay	\times
Optimizer	AdamW
Base Learning rate	1e-3 \rightarrow 1e-5
Linear LR Scaling Divisor	1024
Weight decay	0.05
Momentum	$\beta_1 = 0.9, \beta_2 = 0.999$
Gradient Norm Clip	1.0
Precision	mixed bfloat16
Backend	torch.autocast
Learning rate schedule	cosine decay
Warmup schedule	linear
Warmup epochs	5 \rightarrow 5 (T, S), 1 (B)
End LR	1e-6
Label smoothing	\times
Train Data Augmentation	
RandomResizedCrop	192 \rightarrow 224
Scale	[0.08, 1.0]
Interpolation	bicubic
RandomHorizontalFlip	$p = 0.5$
3-Augment	
Gaussian Blur σ	[0.1, 2.0]
ColorJitter	[0.3, 0.3, 0.3, 0.0]
Normalize	ImageNet-1K statistics
Mixup α	0.8
Cutmix α	1.0
Test Data Augmentation	
Resize	192 \rightarrow 224
Interpolation	bicubic
CenterCrop	192 \rightarrow 224
Normalize	ImageNet-1K statistics

1033
1034
1035
1036
1037
1038
1039
1040
1041
1042
1043
1044
1045
1046
1047
1048
1049
1050
1051
1052
1053
1054
1055
1056
1057
1058
1059
1060
1061
1062
1063
1064
1065
1066
1067
1068
1069
1070
1071
1072
1073
1074
1075
1076
1077
1078
1079

B.4 FINE-TUNING ON VTAB-1K

For fine-tuning models on VTAB-1K we provide the hyperparameters in Table 11. We search for the best learning rate for each dataset by fine-tuning the model 25 times (5 learning rates with 5 seeds each) on the 800 training samples and evaluating them on the 200 validation samples. With the best learning rate, we then train each model 5 times on concatenation of training and validation split, evaluate on the test split and report the average accuracy.

Table 11: Hyperparameters for fine-tuning on VTAB-1K. *For Vim and ViL we group two consecutive blocks for the layer-wise lr decay similar to how ViT considers a pair of attention and MLP block as a single “layer” for the decay.

Parameter	Value
Epochs	50
Batch size	64
Seeds	5
Optimizer	AdamW
Learning rate	[1e-3, 7.5e-4, 5.0e-4, 2.5e-4, 1.0e-4]
Layer-wise lr deca	0.65*
Weight decay	0.05
Momentum	$\beta_1 = 0.9, \beta_2 = 0.999$
Learning rate schedule	linear warmup \rightarrow cosine decay
Warmup epochs	5
Precision	mixed bfloat16
Backend	torch.autocast
Data Augmentation	
Resize	
interpolation	bicubic
size	224x224
Normalize	ImageNet-1K statistics

B.5 ADE20K SEMANTIC SEGMENTATION FINE-TUNING

We fine-tune models on ADE20K (Zhou et al., 2019) using an UperNet (Xiao et al., 2018) head. We follow common practices and fine-tune on 512x512 resolution, where we interpolate the absolute positional embedding from 224x224 to 512x512. For ViTs, we add relative position biases to the attention layers (initialized to 0) (He et al., 2022). Table 12 lists detailed hyperparameters.

Table 12: Hyperparameters for fine-tuning on VTAB-1K. *For ViL we group two consecutive blocks into one similar to how a ViT block consists of a pair of attention and MLP block.

Parameter	Value
Updates	160K
Batch size	16
UperNet	
Auxiliary	
Weight	0.4
Input Block	8*
Dimension	192 (T), 384 (S, B)
Decoder	
Weight	1.0
Input Blocks	[4, 6, 8, 12]*
Dimension	192 (T), 384 (S, B)
Stochastic depth	
Peak rate	0 (T), 0.05 (S), 0.1 (B)
Layer-wise Decay	✓
Optimizer	AdamW
Learning rate	5e-4
Linear LR Scaling Divisor	16
Layer-wise lr decay	0.65*
Weight decay	0.05
Momentum	$\beta_1 = 0.9, \beta_2 = 0.999$
Learning rate schedule	linear warmup \rightarrow cosine decay
Warmup updates	1500
Precision	mixed float16
Backend	torch.autocast
Train Data Augmentation	
RandomResize	
interpolation	bicubic
RandomCrop	
size	512x512
RandomHorizontalFlip	
ColorJitter	0.5
brightness	0.5
contrast	0.5
saturation	0.5
hue	0.25
Normalize	ImageNet-1K statistics
Evaluation	
Stride	341
Multi-scale	
scale factors	[0.75, 1.0, 1.25, 1.5, 1.75]
flip	[True, False]

B.6 DEiT-III REIMPLEMENTATION HYPERPARAMETERS

Table 10 shows detailed hyperparameters used to train DeiT-III-T (reimpl.) from Table 1. Our reimplementation easily outperforms older baselines like DeiT-II-T (+2.7% ImageNet-1K accuracy) and is approximately even with the original on ADE20K (40.1 vs 39.8 on mIoU single-scale, 41.8 vs 42.2 mIoU multi-scale).

Table 13: Hyperparameters for training our reimplementation of DeiT-III-T (Touvron et al., 2022b) on ImageNet-1K. The most significant change is that we reduce the learning rate from $3e-3$ to $1e-3$ as we found this to greatly improve performance. We make minor changes to the protocol such as using AdamW or no gradient clipping as models were stable without it. We follow the best setting from DeiT-III (Touvron et al., 2022b) and pre-train on 192 resolution followed by a short fine-tuning on 224 resolution (indicated by \rightarrow).

Parameter	Value
Epochs	800 \rightarrow 20
Batch size	2048 \rightarrow 1024
Model	
Patch size	16x16
Latent dimension	192
Depth	12
Pooling	[CLS]
Stochastic depth	X
Layerscale	1e-4
Optimizer	AdamW
Base Learning rate	1e-3 \rightarrow 1e-5
Linear LR Scaling Divisor	1024
Weight decay	0.05
Momentum	$\beta_1 = 0.9, \beta_2 = 0.999$
Gradient Norm Clip	X
Precision	mixed bfloat16
Backend	torch.autocast
Learning rate schedule	cosine decay
Warmup schedule	linear
Warmup epochs	5
End LR	1e-6
Label smoothing	X
Train Data Augmentation	
RandomResizedCrop	192 \rightarrow 224
Scale	[0.08, 1.0]
Interpolation	bicubic
RandomHorizontalFlip	$p = 0.5$
3-Augment	
Gaussian Blur σ	[0.1, 2.0]
ColorJitter	[0.3, 0.3, 0.3, 0.0]
Normalize	ImageNet-1K statistics
Mixup α	0.8
Cutmix α	1.0
Test Data Augmentation	
Resize	192 \rightarrow 224
Interpolation	bicubic
CenterCrop	192 \rightarrow 224
Normalize	ImageNet-1K statistics